Quantum Phases in the Honeycomb-Lattice J_1–J_3 Ferro-Antiferromagnetic Model

Shengtao Jiang (蒋晟韬), Steven R. White, and A. L. Chernyshev
Department of Physics and Astronomy, University of California, Irvine, California 92697, USA
(Dated: April 1, 2024)

Using large-scale density-matrix renormalzation group calculations and minimally augmented spin-wave theory, we demonstrate that the phase diagram of the quantum $S = \frac{1}{2}$ J_1–J_3 ferro-antiferromagnetic model on the honeycomb lattice differs dramatically from the classical one. It hosts the double-zigzag and Ising-z phases as unexpected intermediaries between ferromagnetic and zigzag states that are also extended beyond their classical regions of stability. In broad agreement with quantum order-by-disorder arguments, these collinear phases replace the classical spiral state.

Introduction.—Ever since the Anderson's seminal work on the resonating valence-bond state [1], the significant role that can be played by quantum fluctuations in magnets with competing interactions has remained at the forefront of condensed matter physics, inspiring a multitude of quests for exotic states, models that can realize them, and real materials that can host them [2–7]. The elusive spin-liquid states with strongly entangled spins are but one example [2]; others include valence-bond phases with spatial symmetry breaking [8–14], quantum multipolar spin nematics that are quantum analogues of liquid crystals [15–18], and an especially extensive class of unconventional magnetically *ordered* phases that do not appear in the classical solutions of the underlying spin models [19–28]. It is the latter group of phenomena that creates a broader context for the present study.

The ordered phases that are not favored classically but are stabilized in the quantum $S=\frac{1}{2}$ limit have attracted significant attention in the search for Kitaev magnets on the honeycomb lattice [29–32]. Recently, this extensive experimental and theoretical effort has expanded to the Co^{2+} materials [33–46]. It appears that the minimal XXZ-anisotropic J_1–J_3 model with "mixed" ferro-antiferromagnetic (FM-AFM) couplings, given by

$$H = \sum_{n=1,3} \sum_{\langle ij\rangle_n} J_n \left(S_i^x S_j^x + S_i^y S_j^y + \Delta_n S_i^z S_j^z \right), \qquad (1)$$

provides a tantalizingly close description for many of these compounds [43–49], calling for its unbiased study. Here $\langle ij\rangle_{1(3)}$ stands for the first-(third-)neighbor bonds, $J_1 = -1$ is the energy unit, $J_3 > 0$, and $0 \le \Delta_n \le 1$ are the XXZ anisotropies. We note that earlier pre-Kitaev searches for exotic quantum states have focused on a pure AFM J_1–J_2–J_3 honeycomb-lattice model [50–61], motivated by the expectation of stronger fluctuations due to the lattice's low coordination number and by the degeneracies in its classical phase diagram [53].

The model (1) was studied in the 1970s [62], yielding the classical phase diagram reproduced in Fig. 1(a). These phases are independent of Δ_n because all relevant classical states are coplanar. The ground state is FM for small J_3, while zigzag (ZZ) order is preferred for large J_3, and the ferrimagnetic spiral phase (Sp) continuously interpolates between FM and ZZ.

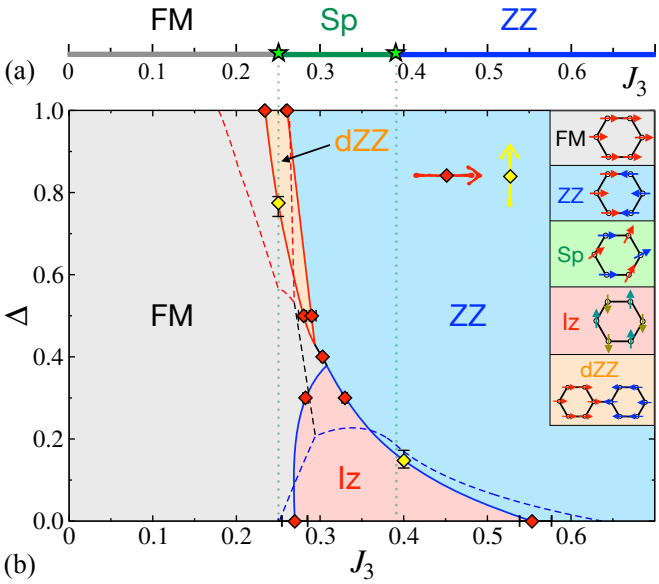

FIG. 1. The classical (a) and quantum (b) phase diagrams of the XXZ J_1^{Δ}–J_3 model (1) with the ferromagnetic (FM), zigzag (ZZ), spiral (Sp), double-zigzag (dZZ), and Ising-z (Iz) phases. The solid lines are phase boundaries interpolating transition points (diamonds) inferred from the DMRG scans along J_3 (red) and Δ (yellow). The vertical and dashed lines are classical and MAGSWT phase boundaries, respectively. Spins are in-plane for all phases except Iz, see also Fig. 2.

In this Letter, we combine density-matrix renormalization group (DMRG) and minimally-augmented spin-wave theory (MAGSWT) to obtain the groundstate phase diagram of the quantum $S = \frac{1}{2}$ model (1). We focus on the *partial* XXZ version of the model (1), with the J_3-term left in the Heisenberg limit, $\Delta_3 = 1$, referred to as the J_1^{Δ}–J_3 model. This choice is motivated by real materials, in which further exchanges tend to be more isotropic [32, 63]. The standard version of the model with equal anisotropies, $\Delta_1 = \Delta_3$, referred to as the *full* XXZ or J_1^{Δ}–J_3^{Δ} model, is considered too.

Phase diagram.—Our phase diagram for the $S = \frac{1}{2}$ J_1^{Δ}–J_3 model is given in Fig. 1(b). In a dramatic deviation from the classical case, we find two unconventional phases stabilized by quantum fluctuations—the double-zigzag (dZZ) and Ising-z (Iz) phases—as intermediary between the FM and ZZ phases. The FM and ZZ phases also extend well beyond their classical regions to com-

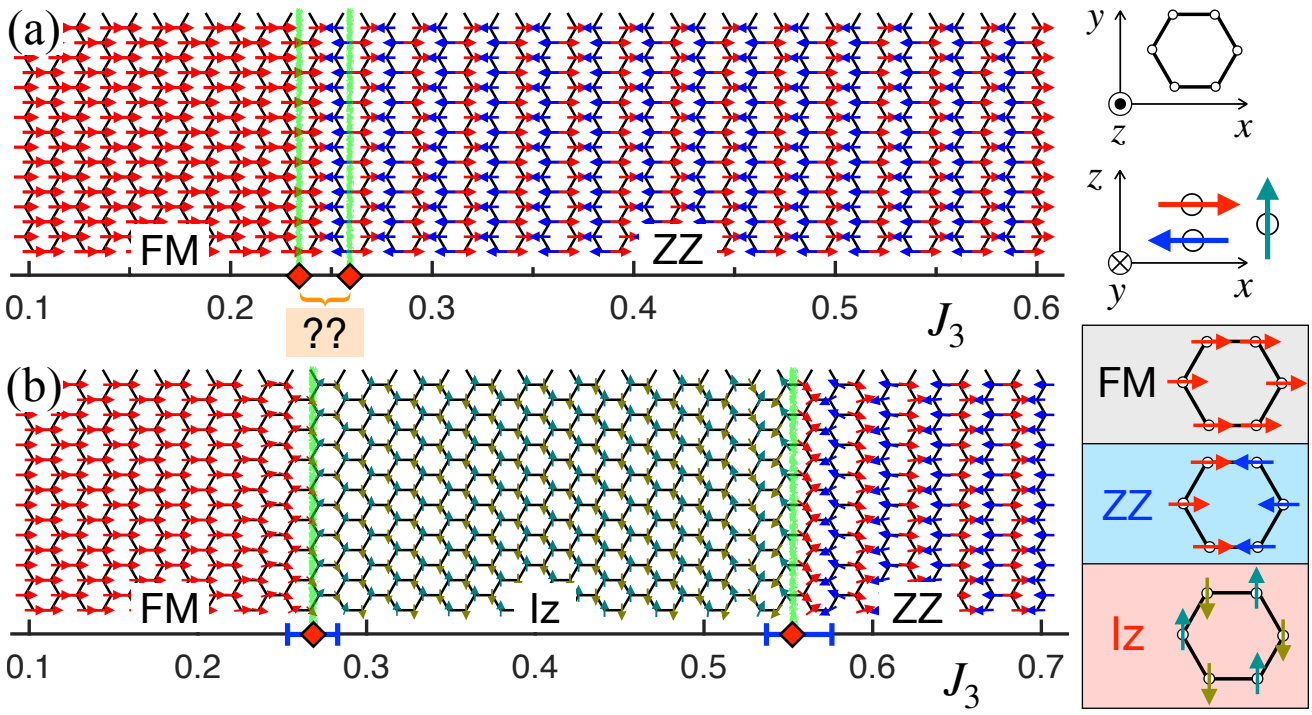

FIG. 2. Long-cylinder scans of the J_1^Δ–J_3 model (1) vs J_3 in the (a) Heisenberg ($\Delta=1$) and (b) XY ($\Delta=0$) limit. The arrows show the local ordered moment $\langle \mathbf{S}_i \rangle$. FM, ZZ, and Iz phases are indicated and transitions are determined as described in text. The honeycomb lattice is in the xy plane while spins shown in the figure are in the xz plane.

pletely supersede the non-collinear classical spiral phase.

The solid lines are phase boundaries interpolating transition points obtained from the DMRG long-cylinder DMRG "scans" by varying J_3 or Δ, as well as from the more precise measurements. The dashed lines are phase boundaries of the same phases obtained by MAGSWT, with both approaches described below.

The qualitative agreement between these approaches is quite remarkable. Both methods produce the classically unstable dZZ and Iz phases, both expand the FM and ZZ phases beyond their classical ranges, and both eliminate the Sp phase. These findings are also in a broad agreement with order-by-disorder arguments [20, 27], which generally favor collinear phases.

We note that recent studies of related models also found the Sp phase to be absent [64, 65]. However, our conclusions on the nature and extent of the quantum phases that replace it differ substantially from theirs. For the details on these differences for the J_1–J_3 and other models, see Ref. [66] and the discussions below.

The $U(1)$-preserving Iz phase, with spins ordered Néel-like along the z axis, has been first discovered in the XY J_1-J_2 AFM-AFM model [60], where Iz order is stabilized solely by quantum effects with no exchange coupling favoring it. In our case, we find the z axis component of the J_3-exchange in the J_1^Δ-J_3 model crucial for stabilizing the Iz phase in a wide range of parameters, see Fig. 1(b). In contrast to Ref. [65], we find only a very narrow Iz phase in the J_1^Δ-J_3^Δ model. The spin-liquid phases in this model [64, 65] are also not supported [66].

The dZZ phase has been recently reported experimentally [43] and found favored by the *bond-dependent* extensions of the XY J_1^Δ–J_3^Δ model [45, 46]. Instead, we find the dZZ phase already in the Heisenberg limit of the principal J_1–J_3 model (1), see Fig. 1(b).

DMRG calculations.—DMRG calculations were performed on the $L_x \times L_y$-site honeycomb-lattice open cylinders of width L_y up to 16 (8 honeycomb cells), using the ITensor library [67]. The majority of the results were obtained on the so-called X-cylinders (XC) [59], in which the first-neighbor bond is horizontal, while both X- and Y-cylinders (YC) were used for more delicate phases [68]. We allow for a spontaneous breaking of the spin $U(1)$ symmetry [69], enabling us to measure the local ordered moment $\langle \mathbf{S}_i \rangle$ instead of the correlation function.

Our main exploratory tool is the long-cylinder "scans," in which one parameter, J_3 or Δ, is varied along the length of the cylinder with L_x up to 40. It provides 1D cuts through the 2D phase diagram [70–73], see Fig. 2, which give approximate phase boundaries. By narrowing parameter ranges of the scans one can determine the boundaries with increased precision, distinguish first- and second-order transitions [15], and uncover hidden phases. In cases when the phase boundary is less obvious, we utilize the fixed parameter (non-scan) calculations on clusters up to 16×16, with the aspect ratio that closely approximates the 2D thermodynamic limit [74].

In Fig. 2, we present two long-cylinder scans for the J_1^Δ–J_3 model (1), one in the Heisenberg limit, $\Delta = 1$, and the other in the XY limit, $\Delta = 0$, vs J_3. In the

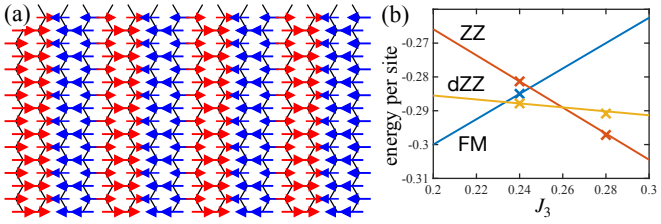

FIG. 3. (a) Ordered moments in the 16×16 non-scan cluster for J_3=0.24, showing dZZ pattern. (b) Energies of the three competing phases vs J_3, crosses are DMRG results and higher-energy states are metastable. Lines are extrapolated energies, $\langle\psi_i|H(J_3)|\psi_i\rangle$, where ψ_i are the three states at $J_3=0.24$.

Heisenberg limit, Fig. 2(a), the transition from FM to ZZ is very sharp and FM phase seems to terminate right at the classical boundary of this state, $J_3^{cl}=0.25$. However, one would expect that the FM phase should retreat from this boundary, as the competing ZZ state is fluctuating in the Heisenberg limit, while the FM state is exact. The subsequent analysis reveals a hidden intermediate dZZ state, discussed next. We note that the scan calculation in Fig. 2(a) misses it not only due to the narrow region of the dZZ phase, but also because of the high symmetry of the model in the Heisenberg limit, which requires additional effort to avoid metastable states.

Fig. 2(b) for the XY limit shows transitions from the FM to Iz and from Iz to ZZ vs J_3. By using scans in the narrower ranges of J_3, we verify that the spiral-like spin patterns in the transition regions in Fig. 2(b) are proximity effects of the neighboring phases, not additional phases. The phase boundaries shown in Fig. 2(b) and used in the phase diagram in Fig. 1(b) are the crossing points of the order parameters vs J_3 [66]. The error bars are the width of the transition region in the scans, where a discontinuous transition is assigned a width equal to the parameter change over one lattice spacing.

In the Heisenberg limit, the three states, FM, dZZ, and ZZ, compete in the proximity of the classical FM boundary $J_3=0.25$. Because of the high spin-symmetry of the model, and depending on the initial state, all three can be stabilized in the non-scan DMRG simulations, such as the one shown in Fig. 3(a) for $J_3=0.24$ in the 16×16 cluster. As is shown in Fig. 3(b), the energy of the dZZ is the lowest, with the FM and ZZ being metastable, suggesting that the transitions between the corresponding phases are first order. To identify their phase boundaries, we compare the energies of these three states as a function of J_3 using extrapolations based on the spin-spin correlations extracted at $J_3=0.24$ from the center of the cluster for each of the states. While the FM line is exact in this limit, the extrapolated energies for ZZ and dZZ are also very close to the ones given by a direct DMRG calculation at a different value of J_3, justifying the analysis, see Fig. 3(b). The dZZ phase is found to be confined between J_3=0.2333 and 0.2596.

The lower spin-symmetry away from the Heisenberg limit helps to reveal the dZZ phase more readily, see

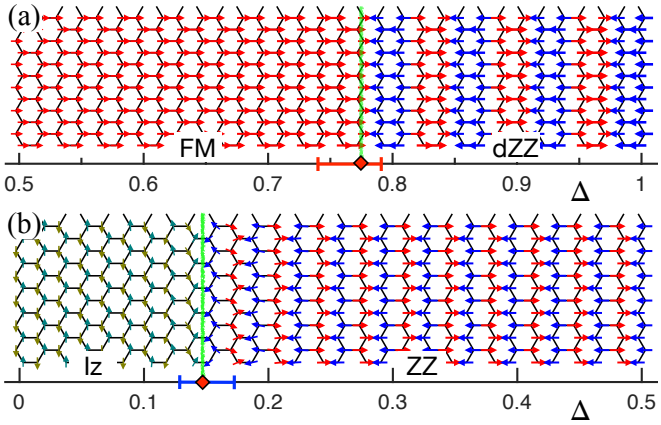

FIG. 4. Long-cylinder Δ-scans of the J_1^{Δ}–J_3 model (1) for (a) $J_3=0.25$ and (b) $J_3=0.4$. Notations are as in Fig. 2.

Fig. 4(a) for a long-cylinder scan along the Δ axis and fixed $J_3=0.25$, confirming the presence of this phase in an extended region of the phase diagram in Fig. 1. A similar Δ-scan for $J_3=0.4$ in Fig. 4(b) compliments the J_3-scans in establishing boundaries of the Iz phase.

By using a combination of the narrower ranges of the scans and fixed-parameter non-scans, we find that the dZZ phase persists somewhat below $\Delta=0.5$ while the Iz phase ends close to $\Delta=0.4$, where the FM-to-ZZ transition appears to be direct, see Fig. 1 and [66]. Although we cannot completely rule out the Iz state for $\Delta=0.4$, it must be extremely narrow if it exists.

Minimally-augmented spin-wave theory.—The standard SWT is successful at accounting for quantum effects in the ordered states [75], but cannot describe either the ordered phases that are not classically stable, or the shifts of the phase boundaries by quantum fluctuations. An analytical approach to address this problem, originally proposed for the classically unstable field-induced states in the transverse-field Ising and frustrated Heisenberg models [76–78], can be successfully applied here.

The method consists of introducing a local field in the direction of the ordered moment $\mathbf{n}_i$ for the proposed (unstable) classical spin configurations, leading to a shift of the chemical potential in the bosonic SWT language

$$\delta\mathcal{H}=\mu\sum_i(S-\mathbf{S}_i\cdot\mathbf{n}_i)=\mu\sum_i a_i^\dagger a_i, \qquad (2)$$

while leaving the classical energy of the state unchanged. The *minimal* value of μ is chosen to ensure stability of the spectrum, i.e., that the squares of all eigenvalues of the SWT matrix are positive definite. Then, the energy of the proposed spin state, $\mathcal{E}=E_{cl}+\delta E$, with the $1/S$-correction to the groundstate energy δE, is well-defined and can be compared with the energies of the competing states calculated to the same $O(S)$ order.

The power of the method, coined as the *minimally augmented SWT* (MAGSWT), is not only in its simplicity, but in the form of Eq. (2), which guarantees that its contribution to the Hamiltonian is positive for $\mu>0$. In turn, this implies that the so-obtained groundstate energy $\mathcal{E}$ is

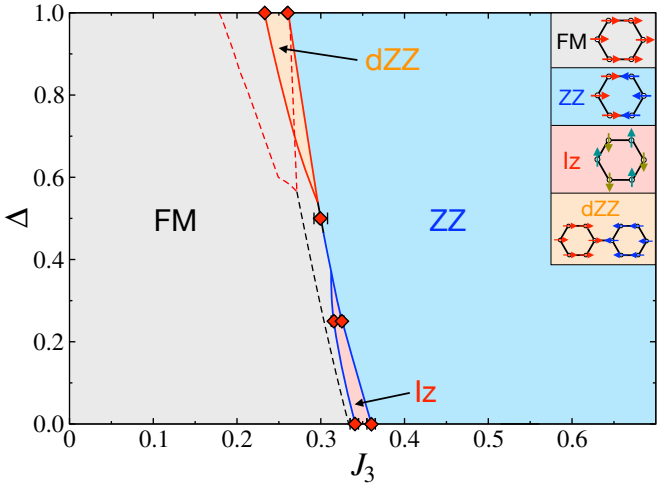

FIG. 5. The quantum $S=\frac{1}{2}$ phase diagrams of the full XXZ J_1^Δ–J_3^Δ model (1), c.f. Fig. 1(b). See text.

an *upper bound* for the energy of the suggested spin state to the order $O(S)$. This method allows one to consider the phase beyond its classical range of stability and inspect states that are classically not competitive, but can lower their energy due to quantum fluctuations. The new phase boundaries are determined from the crossings of the energies $\mathcal{E}$ for the competing phases as a function of the varied parameter(s).

We note that MAGSWT may not be applied to an arbitrary classically-unstable state [78], with the absence of the linear-bosonic terms in the $1/S$-expansion for a given state being a sufficient criterion of its applicability.

MAGSWT results.—In case of the XXZ J_1^Δ–J_3 model (1), all four competing phases of interest are collinear, which guarantees the absence of the linear-bosonic terms, while the non-collinear Sp state is not the subject of MAGSWT, as it corresponds to a minimum of the classical energy in its entire possible range of existence.

The technical procedure of extracting minimal μ vs J_3 and Δ for each phase is discussed in Ref. [66]. We note that the limiting XY and Heisenberg cases and select momenta are useful for obtaining analytical expressions for $\mu(J_3,\Delta)$, eliminating the need of a numerical scan of the momentum space for spectrum instabilities. With that, the energy surfaces $\mathcal{E}(J_3,\Delta)$ are readily obtained for each phase and the MAGSWT phase boundaries are drawn from the intersections of such surfaces.

The resulting phase boundaries are shown in Fig. 1(b) by the dashed lines. Most, if not all, of the features already discussed above are present. The noncollinear Sp phase is not effective at benefiting from quantum fluctuations, in agreement with the order-by-disorder arguments [20], and is wiped out. The classically-unstable dZZ and Iz phases are extensive and both FM and ZZ expand beyond their classical borders. A close quantitative agreement with the DMRG phase boundaries can also be observed, with most discrepancies concerning the borders of the less-fluctuating FM phase [66]. Otherwise, the entire picture for the J_1^Δ–J_3 model in Fig. 1(b) is in rather astonishing agreement with the numerical data.

The J_1^Δ–J_3^Δ model.—The phase diagram of the full XXZ model (1) with equal anisotropies in both terms, obtained using the same methods as described above, is presented in Fig. 5. It repeats most of the trends of the partial XXZ model in Fig. 1(b), such as the absence of the Sp phase, expansion of the FM and ZZ, and the presence of the two unconventional phases, Iz and dZZ.

In contrast to the recent studies [64, 65], our results do not support the proposed spin-liquid states in the Heisenberg [65], or strongly-anisotropic ($\Delta=0.25$) nearly XY [64] limits. The J_3-width of the quantum Iz phase in the same XY limit ($\Delta=0$) is also an order of magnitude narrower in our case than the one suggested in [65].

While the first of the quantum phases, dZZ, missed by the previous works due to small cluster sizes or an approximate nature of their approaches [65], is nearly the same in the partial and full XXZ models in Fig. 1(b) and Fig. 5, respectively, the Iz phase is substantially more tenuous. In fact, the initial DMRG scans have shown a direct FM-ZZ transition, with some possible narrow intermediate state. Dedicated non-scans in that region did uncover short-range correlations in both XC and YC clusters [66], not unlike the ones reported in Ref. [64]. However, these spin-liquid-suspects either order on the cylinder width increase (XC), or indicate a sufficiently robust Iz order in the range of J_3=0.315-0.325 for $\Delta=0.25$ and J_3=0.34-0.36 for $\Delta=0$, see [66].

It is worth noting that MAGSWT in the XY limit of the full XXZ model shows a close, but insufficient, competition of the strongly fluctuating Iz phase, rendering it absent from its version of the phase diagram in Fig. 5.

Summary.—In this letter, we have studied the emergence of the quantum phases that are not stable classically within a simple model of great current interest. We have combined state-of-the-art DMRG and analytical approaches to obtain conclusive phase diagrams of this model. It is established beyond any reasonable doubt that the two unconventional quantum phases occupy a significant portion of this diagram, with the known phases also extending well beyond their classical regions and completely replacing the less-fluctuating non-collinear phase. The results of the analytical MAGSWT approach are shown to be in a close accord with the numerical DMRG data, providing additional insights into the energetics of the quantum stabilization of the non-classical phases and offering a systematic path for the explorations of similar models.

The proposed phase diagrams have direct relevance to a group of novel materials and provide important guidance to the ongoing theoretical and experimental searches of the unconventional quantum states.

Acknowledgments.—We are sincerely thankful to Arun Paramekanti for several important discussions and numerous exchanges. We are grateful to Ciarán Hickey, Si-

mon Trebst, and Yoshito Watanabe for the kind remarks and useful conversations. The work of S. J. and S. R. W. was supported by the NSF through grant DMR-2110041. The inception of the paper, key analysis, and analytical and numerical calculations using MAGSWT by A. L. C. were supported by the U.S. Department of Energy, Office of Science, Basic Energy Sciences under Award No. DE-SC0021221.

[1] P. Anderson, Resonating valence bonds: A new kind of insulator?, Mater. Res. Bull. **8**, 153 (1973).
[2] L. Balents, Spin liquids in frustrated magnets, Nature **464**, 199 (2010).
[3] M. R. Norman, Colloquium: Herbertsmithite and the search for the quantum spin liquid, Rev. Mod. Phys. **88**, 041002 (2016).
[4] Y. Zhou, K. Kanoda, and T.-K. Ng, Quantum spin liquid states, Rev. Mod. Phys. **89**, 025003 (2017).
[5] J. Knolle and R. Moessner, A field guide to spin liquids, Annu. Rev. Condens. Matter Phys. **10**, 451 (2019).
[6] A. Kitaev, Anyons in an exactly solved model and beyond, Ann. Phys. **321**, 2 (2006).
[7] L. Capriotti, F. Becca, A. Parola, and S. Sorella, Resonating Valence Bond Wave Functions for Strongly Frustrated Spin Systems, Phys. Rev. Lett. **87**, 097201 (2001).
[8] V. Zapf, M. Jaime, and C. D. Batista, Bose-Einstein condensation in quantum magnets, Rev. Mod. Phys. **86**, 563 (2014).
[9] M. Mambrini, A. Läuchli, D. Poilblanc, and F. Mila, Plaquette valence-bond crystal in the frustrated Heisenberg quantum antiferromagnet on the square lattice, Phys. Rev. B **74**, 144422 (2006).
[10] S.-S. Gong, W. Zhu, D. N. Sheng, O. I. Motrunich, and M. P. A. Fisher, Plaquette Ordered Phase and Quantum Phase Diagram in the Spin-$\frac{1}{2}$ J_1-J_2 Square Heisenberg Model, Phys. Rev. Lett. **113**, 027201 (2014).
[11] K. Kodama, M. Takigawa, M. Horvatić, C. Berthier, H. Kageyama, Y. Ueda, S. Miyahara, F. Becca, and F. Mila, Magnetic Superstructure in the Two-Dimensional Quantum Antiferromagnet $SrCu_2(BO_3)_2$, Science **298**, 395 (2002).
[12] Y. H. Matsuda, N. Abe, S. Takeyama, H. Kageyama, P. Corboz, A. Honecker, S. R. Manmana, G. R. Foltin, K. P. Schmidt, and F. Mila, Magnetization of $SrCu_2(BO_3)_2$ in Ultrahigh Magnetic Fields up to 118 T, Phys. Rev. Lett. **111**, 137204 (2013).
[13] M. Jaime, R. Daou, S. A. Crooker, F. Weickert, A. Uchida, A. E. Feiguin, C. D. Batista, H. A. Dabkowska, and B. D. Gaulin, Magnetostriction and magnetic texture to 100.75 Tesla in frustrated $SrCu_2(BO_3)_2$, Proc. Natl. Acad. Sci. U.S.A. **109**, 12404 (2012).
[14] F. Ferrari, S. Bieri, and F. Becca, Competition between spin liquids and valence-bond order in the frustrated spin-$\frac{1}{2}$ Heisenberg model on the honeycomb lattice, Phys. Rev. B **96**, 104401 (2017).
[15] S. Jiang, J. Romhányi, S. R. White, M. E. Zhitomirsky, and A. L. Chernyshev, Where is the Quantum Spin Nematic?, Phys. Rev. Lett. **130**, 116701 (2023).
[16] M. E. Zhitomirsky and H. Tsunetsugu, Magnon pairing in quantum spin nematic, EPL (Europhysics Letters) **92**, 37001 (2010).
[17] K. Penc and A. M. Läuchli, in *Introduction to Frustrated Magnetism: Materials, Experiments, Theory*, edited by C. Lacroix, P. Mendels, and F. Mila (Springer-Verlag Berlin Heidelberg, 2011) Chap. Spin Nematic Phases in Quantum Spin Systems, p. 331.
[18] Y. Kohama, H. Ishikawa, A. Matsuo, K. Kindo, N. Shannon, and Z. Hiroi, Possible observation of quantum spin-nematic phase in a frustrated magnet, Proc. Natl. Acad. Sci. U.S.A. **116**, 10686 (2019).
[19] C. L. Henley, Ordering by disorder: Ground-state selection in fcc vector antiferromagnets, J. Appl. Phys. **61**, 3962 (1987).
[20] C. L. Henley, Ordering due to disorder in a frustrated vector antiferromagnet, Phys. Rev. Lett. **62**, 2056 (1989).
[21] O. A. Starykh, Unusual ordered phases of highly frustrated magnets: a review, Rep. Prog. Phys. **78**, 052502 (2015).
[22] A. W. C. Wong, Z. Hao, and M. J. P. Gingras, Ground state phase diagram of generic XY pyrochlore magnets with quantum fluctuations, Phys. Rev. B **88**, 144402 (2013).
[23] K. A. Ross, L. Savary, B. D. Gaulin, and L. Balents, Quantum excitations in quantum spin ice, Phys. Rev. X **1**, 021002 (2011).
[24] J. G. Rau and M. J. Gingras, Frustrated quantum rare-earth pyrochlores, Annu. Rev. Condens. Matter Phys. **10**, 357 (2019).
[25] A. M. Hallas, J. Gaudet, and B. D. Gaulin, Experimental Insights into Ground-State Selection of Quantum XY Pyrochlores, Annu. Rev. Condens. Matter Phys. **9**, 105 (2018).
[26] J. G. Rau, R. Moessner, and P. A. McClarty, Magnon interactions in the frustrated pyrochlore ferromagnet $Yb_2Ti_2O_7$, Phys. Rev. B **100**, 104423 (2019).
[27] J. G. Rau, P. A. McClarty, and R. Moessner, Pseudo-Goldstone Gaps and Order-by-Quantum Disorder in Frustrated Magnets, Phys. Rev. Lett. **121**, 237201 (2018).
[28] R. Schick, O. Götze, T. Ziman, R. Zinke, J. Richter, and M. E. Zhitomirsky, Ground-state selection by magnon interactions in a fcc antiferromagnet, Phys. Rev. B **106**, 094431 (2022).
[29] W. Witczak-Krempa, G. Chen, Y. B. Kim, and L. Balents, Correlated Quantum Phenomena in the Strong Spin-Orbit Regime, Annu. Rev. Condens. Matter Phys. **5**, 57 (2014).
[30] R. Schaffer, E. K.-H. Lee, B.-J. Yang, and Y. B. Kim, Recent progress on correlated electron systems with strong spin-orbit coupling, Rep. Prog. Phys. **79**, 094504 (2016).
[31] J. G. Rau, E. K.-H. Lee, and H.-Y. Kee, Spin-Orbit Physics Giving Rise to Novel Phases in Correlated Systems: Iridates and Related Materials, Annu. Rev. Condens. Matter Phys. **7**, 195 (2016).
[32] S. M. Winter, A. A. Tsirlin, M. Daghofer, J. van den Brink, Y. Singh, P. Gegenwart, and R. Valentí, Models and materials for generalized Kitaev magnetism, J. Phys. Condens. Matter **29**, 493002 (2017).
[33] H. Liu and G. Khaliullin, Pseudospin exchange interactions in d^7 cobalt compounds: Possible realization of the Kitaev model, Phys. Rev. B **97**, 014407 (2018).
[34] H. Liu, J. Chaloupka, and G. Khaliullin, Kitaev Spin

Liquid in 3*d* Transition Metal Compounds, Phys. Rev. Lett. **125**, 047201 (2020).
[35] X. Zhang, Y. Xu, T. Halloran, R. Zhong, C. Broholm, R. Cava, N. Drichko, and N. Armitage, A magnetic continuum in the cobalt-based honeycomb magnet $BaCo_2(AsO_4)_2$, Nat. Mater. **22**, 58 (2023).
[36] R. Zhong, T. Gao, N. P. Ong, and R. J. Cava, Weak-field induced nonmagnetic state in a Co-based honeycomb, Sci. Adv. **6**, eaay6953 (2020).
[37] H. S. Nair, J. M. Brown, E. Coldren, G. Hester, M. P. Gelfand, A. Podlesnyak, Q. Huang, and K. A. Ross, Short-range order in the quantum XXZ honeycomb lattice material $BaCo_2(PO_4)_2$, Phys. Rev. B **97**, 134409 (2018).
[38] X. Wang, R. Sharma, P. Becker, L. Bohatý, and T. Lorenz, Single-crystal study of the honeycomb XXZ magnet $BaCo_2(PO_4)_2$ in magnetic fields, Phys. Rev. Mater. **7**, 024402 (2023).
[39] H. Yang, C. Kim, Y. Choi, J. H. Lee, G. Lin, J. Ma, M. Kratochvílová, P. Proschek, E.-G. Moon, K. H. Lee, Y. S. Oh, and J.-G. Park, Significant thermal Hall effect in the 3*d* cobalt Kitaev system $Na_2Co_2TeO_6$, Phys. Rev. B **106**, L081116 (2022).
[40] W. Yao, Y. Zhao, Y. Qiu, C. Balz, J. R. Stewart, J. W. Lynn, and Y. Li, Magnetic ground state of the Kitaev $Na_2Co_2TeO_6$ spin liquid candidate, Phys. Rev. Res. **5**, L022045 (2023).
[41] M. Songvilay, J. Robert, S. Petit, J. A. Rodriguez-Rivera, W. D. Ratcliff, F. Damay, V. Balédent, M. Jiménez-Ruiz, P. Lejay, E. Pachoud, A. Hadj-Azzem, V. Simonet, and C. Stock, Kitaev interactions in the Co honeycomb antiferromagnets $Na_3Co_2SbO_6$ and $Na_2Co_2TeO_6$, Phys. Rev. B **102**, 224429 (2020).
[42] X. Li, Y. Gu, Y. Chen, V. O. Garlea, K. Iida, K. Kamazawa, Y. Li, G. Deng, Q. Xiao, X. Zheng, Z. Ye, Y. Peng, I. A. Zaliznyak, J. M. Tranquada, and Y. Li, Giant Magnetic In-Plane Anisotropy and Competing Instabilities in $Na_3Co_2SbO_6$, Phys. Rev. X **12**, 041024 (2022).
[43] L.-P. Regnault, C. Boullier, and J. Lorenzo, Polarized-neutron investigation of magnetic ordering and spin dynamics in $BaCo_2(AsO_4)_2$ frustrated honeycomb-lattice magnet, Heliyon **4**, e00507 (2018).
[44] S. Das, S. Voleti, T. Saha-Dasgupta, and A. Paramekanti, XY magnetism, Kitaev exchange, and long-range frustration in the $J_{\rm eff} = \frac{1}{2}$ honeycomb cobaltates, Phys. Rev. B **104**, 134425 (2021).
[45] P. A. Maksimov, A. V. Ushakov, Z. V. Pchelkina, Y. Li, S. M. Winter, and S. V. Streltsov, Ab initio guided minimal model for the "Kitaev" material $BaCo_2(AsO_4)_2$: Importance of direct hopping, third-neighbor exchange, and quantum fluctuations, Phys. Rev. B **106**, 165131 (2022).
[46] T. Halloran, F. Desrochers, E. Z. Zhang, T. Chen, L. E. Chern, Z. Xu, B. Winn, M. Graves-Brook, M. B. Stone, A. I. Kolesnikov, Y. Qiu, R. Zhong, R. Cava, Y. B. Kim, and C. Broholm, Geometrical frustration versus Kitaev interactions in $BaCo_2(AsO_4)_2$, Proc. Natl. Acad. Sci. U.S.A. **120**, e2215509119 (2023).
[47] P. A. Maksimov and A. L. Chernyshev, Rethinking α-$RuCl_3$, Phys. Rev. Res. **2**, 033011 (2020).
[48] L. Regnault and J. Rossat-Mignod, Phase transitions in quasi two-dimensional planar magnets, in *Magnetic Properties of Layered Transition Metal Compounds* (Springer, 1990) pp. 271–321.
[49] A. L. Chernyshev, M. E. Zhitomirsky, N. Martin, and L.-P. Regnault, Lifetime of Gapped Excitations in a Collinear Quantum Antiferromagnet, Phys. Rev. Lett. **109**, 097201 (2012).
[50] Z. Weihong, J. Oitmaa, and C. J. Hamer, Second-order spin-wave results for the quantum XXZ and XY models with anisotropy, Phys. Rev. B **44**, 11869 (1991).
[51] R. R. P. Singh, Z. Weihong, C. J. Hamer, and J. Oitmaa, Dimer order with striped correlations in the J_1-J_2 Heisenberg model, Phys. Rev. B **60**, 7278 (1999).
[52] J. Fouet, P. Sindzingre, and C. Lhuillier, An investigation of the quantum J_1-J_2-J_3 model on the honeycomb lattice, Eur. Phys. J. B **20**, 241 (2001).
[53] A. Mulder, R. Ganesh, L. Capriotti, and A. Paramekanti, Spiral order by disorder and lattice nematic order in a frustrated Heisenberg antiferromagnet on the honeycomb lattice, Phys. Rev. B **81**, 214419 (2010).
[54] J. Oitmaa and R. R. P. Singh, Phase diagram of the $J_1 - J_2 - J_3$ Heisenberg model on the honeycomb lattice: A series expansion study, Phys. Rev. B **84**, 094424 (2011).
[55] D. C. Cabra, C. A. Lamas, and H. D. Rosales, Quantum disordered phase on the frustrated honeycomb lattice, Phys. Rev. B **83**, 094506 (2011).
[56] C. N. Varney, K. Sun, V. Galitski, and M. Rigol, Kaleidoscope of Exotic Quantum Phases in a Frustrated XY Model, Phys. Rev. Lett. **107**, 077201 (2011).
[57] P. H. Y. Li, R. F. Bishop, and C. E. Campbell, Phase diagram of a frustrated spin-$\frac{1}{2}$ J_1-J_2 XXZ model on the honeycomb lattice, Phys. Rev. B **89**, 220408(R) (2014).
[58] S.-S. Gong, D. N. Sheng, O. I. Motrunich, and M. P. A. Fisher, Phase diagram of the spin-$\frac{1}{2}$ J_1-J_2 Heisenberg model on a honeycomb lattice, Phys. Rev. B **88**, 165138 (2013).
[59] Z. Zhu, D. A. Huse, and S. R. White, Weak Plaquette Valence Bond Order in the S=1/2 Honeycomb J_1-J_2 Heisenberg Model, Phys. Rev. Lett. **110**, 127205 (2013).
[60] Z. Zhu, D. A. Huse, and S. R. White, Unexpected z-Direction Ising Antiferromagnetic Order in a Frustrated Spin-1/2 $J_1 - J_2$ XY Model on the Honeycomb Lattice, Phys. Rev. Lett. **111**, 257201 (2013).
[61] R. Ganesh, J. van den Brink, and S. Nishimoto, Deconfined Criticality in the Frustrated Heisenberg Honeycomb Antiferromagnet, Phys. Rev. Lett. **110**, 127203 (2013).
[62] E. Rastelli, A. Tassi, and L. Reatto, Non-simple magnetic order for simple Hamiltonians, Physica B+C **97**, 1 (1979).
[63] S. M. Winter, Y. Li, H. O. Jeschke, and R. Valentí, Challenges in design of Kitaev materials: Magnetic interactions from competing energy scales, Phys. Rev. B **93**, 214431 (2016).
[64] A. Bose, M. Routh, S. Voleti, S. K. Saha, M. Kumar, T. Saha-Dasgupta, and A. Paramekanti, Proximate Dirac spin liquid in the J_1-J_3 XXZ model for honeycomb cobaltates, arXiv:2212.13271 (2022).
[65] Y. Watanabe, S. Trebst, and C. Hickey, Frustrated Ferromagnetism of Honeycomb Cobaltates: Incommensurate Spirals, Quantum Disordered Phases, and Out-of-Plane Ising Order, arXiv:2212.14053 (2022).
[66] See Supplemental Material at [], which includes Refs. [79, 80], for the details on the DMRG calculations, additional results, and details of the analytical MAGSWT formalism.
[67] M. Fishman, S. R. White, and E. M. Stoudenmire, The itensor software library for tensor network calculations, SciPost Phys. Codebases , 4 (2022).

[68] We typically perform 16 sweeps and reach a maximum bond dimension of $m \sim 3000$ to ensure good convergence with the truncation error of $\mathcal{O}(10^{-5})$.

[69] Such symmetry breaking in DMRG mimics the 2D system, see Sec. I of the SI in Ref. [81].

[70] Z. Zhu and S. R. White, Spin liquid phase of the $S = \frac{1}{2}$ J_1–J_2 Heisenberg model on the triangular lattice, Phys. Rev. B **92**, 041105(R) (2015).

[71] Z. Zhu, D. A. Huse, and S. R. White, Unexpected z-Direction Ising Antiferromagnetic Order in a Frustrated Spin-1/2 J_1–J_2 XY Model on the Honeycomb Lattice, Phys. Rev. Lett. **111**, 257201 (2013).

[72] Z. Zhu, P. A. Maksimov, S. R. White, and A. L. Chernyshev, Disorder-Induced Mimicry of a Spin Liquid in $YbMgGaO_4$, Phys. Rev. Lett. **119**, 157201 (2017).

[73] Z. Zhu, P. A. Maksimov, S. R. White, and A. L. Chernyshev, Topography of Spin Liquids on a Triangular Lattice, Phys. Rev. Lett. **120**, 207203 (2018).

[74] S. R. White and A. L. Chernyshev, Neél Order in Square and Triangular Lattice Heisenberg Models, Phys. Rev. Lett. **99**, 127004 (2007).

[75] M. E. Zhitomirsky and A. L. Chernyshev, Colloquium: Spontaneous magnon decays, Rev. Mod. Phys. **85**, 219 (2013).

[76] S. Wenzel, T. Coletta, S. E. Korshunov, and F. Mila, Evidence for Columnar Order in the Fully Frustrated Transverse Field Ising Model on the Square Lattice, Phys. Rev. Lett. **109**, 187202 (2012).

[77] T. Coletta, S. E. Korshunov, and F. Mila, Semiclassical evidence of columnar order in the fully frustrated transverse-field Ising model on the square lattice, Phys. Rev. B **90**, 205109 (2014).

[78] T. Coletta, M. E. Zhitomirsky, and F. Mila, Quantum stabilization of classically unstable plateau structures, Phys. Rev. B **87**, 060407(R) (2013).

[79] T. Holstein and H. Primakoff, Field dependence of the intrinsic domain magnetization of a ferromagnet, Phys. Rev. **58**, 1098 (1940).

[80] J. Colpa, Diagonalization of the quadratic boson hamiltonian, Physica A: Statistical Mechanics and its Applications **93**, 327 (1978).

[81] S. Jiang, D. J. Scalapino, and S. R. White, Ground-state phase diagram of the t-t'-J model, Proc. Natl. Acad. Sci. U.S.A. **118** (2021).

Quantum Phases in the Honeycomb-Lattice J_1–J_3 Ferro-Antiferromagnetic Model: Supplemental Material

Shengtao Jiang (蒋晟韬), Steven R. White, and A. L. Chernyshev
Department of Physics and Astronomy, University of California, Irvine, California 92697, USA
(Dated: April 1, 2024)

I. PHASE BOUNDARIES FROM THE DMRG SCANS

Here we illustrate how we determine the approximate phase boundaries and corresponding error bars from the DMRG scans. In Figure S1, we show the in-plane, $|\langle S_i^x\rangle|$, and out-of-plane, $|\langle S_i^z\rangle|$, ordered moments along the DMRG J_3-scan in Fig. 2(b) of the main text. Spins in the FM and ZZ phases are along the x axis, while in the Iz phase they order along the z axis. The transition points are chosen as the crossing points of their order parameters. Error bars are either the distance to the inflection points of the order-parameter curves or a minimum of one step of the scan (one column of the cylinder) for sharper transitions.

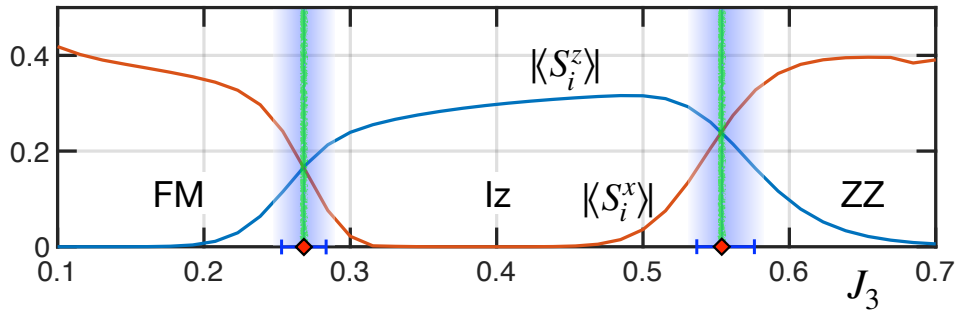

FIG. S1. $|\langle S_i^z\rangle|$ and $|\langle S_i^x\rangle|$ along the length of a 16×40 cylinder in a DMRG scan vs J_3 for the $\Delta=0$ limit of the J_1^{Δ}–J_3 model. The crossing points are the phase boundaries and the shaded regions are the error bars.

II. PROXIMITY EFFECT IN THE SCANS AND THE ABSENCE OF AN SPIRAL PHASE

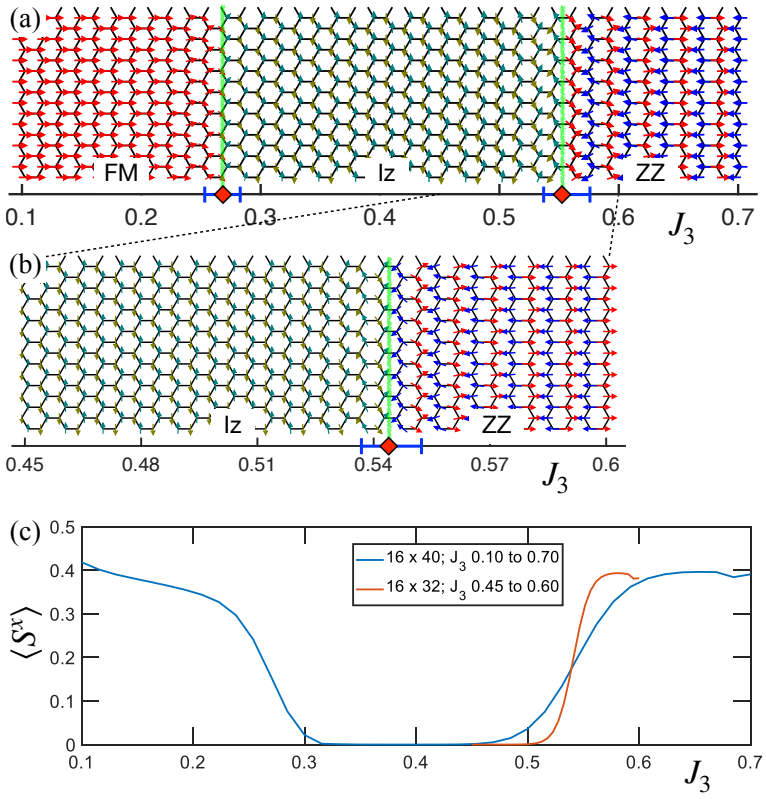

FIG. S2. Results for the J_1^{Δ}–J_3 model at $\Delta=0$. (a) The J_3-scan from Fig. 2(b) of the main text. (b) The "zoom-in" J_3-scan of the Iz-to-ZZ transition region in the 16×32 cylinder. (c) The column-averaged $\langle S^x\rangle$ vs J_3 for the scans in (a) and (b).

In some DMRG scans, such as the one in Fig. 2(b) of the main text, reproduced in Fig. S2(a), spins at the boundary between the Iz and other phases appear to form a spiral pattern. To rule out an additional intermediate spiral phase, we perform a scan in a smaller range of the varied parameter ("zoom-in" scan) to observe the boundary region closer. In Fig. S2(b) we focus on the transition region between the Iz phase and the ZZ phase. If the spiral phase would exist, it would become wider in such a scan. In Fig. S2(b), the transition region has the same width (about ten columns) as in Fig. S2(a), with the transition getting sharper for the smaller gradient of J_3, see Fig. S2(c), strongly suggesting the absence of any intermediate phase in the thermodynamic limit. In the non-scan calculation at J_3=0.55 we also do not find the spiral phase. This analysis clearly shows that the spiral-like pattern in the scans is due to a proximity effect at the phase boundary. Similar verifications were carried out for all suspicious phases in all scans.

III. OTHER DMRG SCANS FOR THE PARTIAL XXZ J_1^Δ–J_3 MODEL

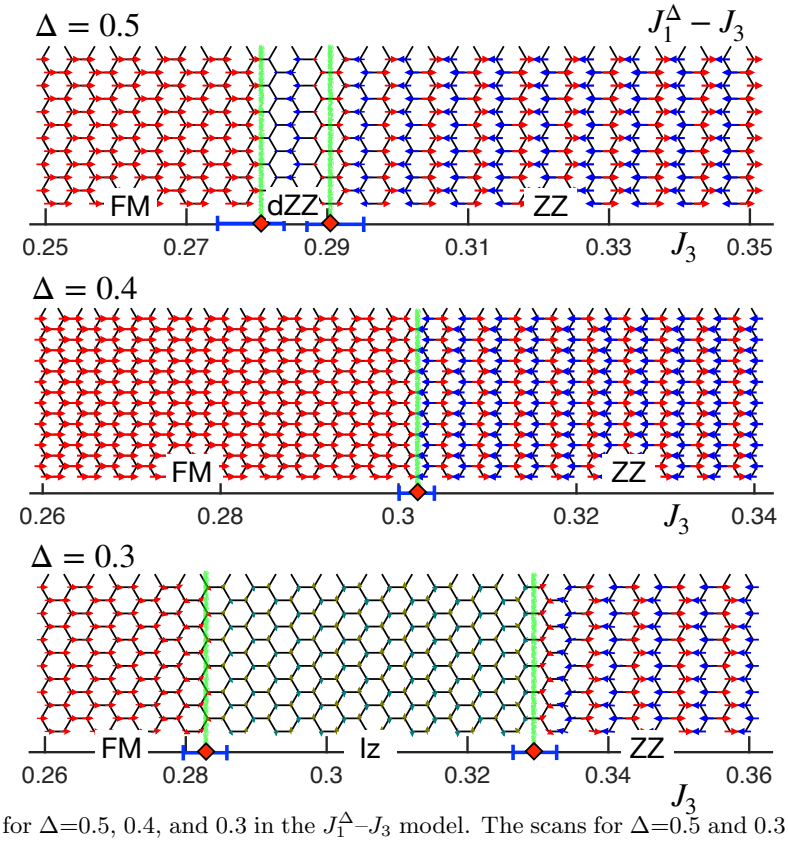

FIG. S3. DMRG J_3-scans for Δ=0.5, 0.4, and 0.3 in the J_1^Δ–J_3 model. The scans for Δ=0.5 and 0.3 are on the 12×32 cylinders while the Δ=0.4 scan is on the 16×40 cylinder.

In Fig. S3, we show additional J_3-scans that are used to construct the phase diagram of the J_1^Δ–J_3 model in Fig. 1(b) of the main text. In each scan, approximate transition boundaries with error bars are indicated. In the $\Delta=0.5$ scan, we observe a narrow phase intervening between FM and ZZ, which is identified as the dZZ phase using non-scan calculations in the region of J_3 from 0.28 to 0.29 (not shown). The $\Delta=0.4$ scan in Fig. S3 shows a direct transition from FM to ZZ. The non-scans using smaller clusters in the vicinity of $J_3=0.3$ have initially suggested a spin-liquid (SL) state discussed below, which turns into ZZ order in the larger non-scan clusters. The $\Delta=0.3$ scan is similar to Fig. 2(b) of the main text with an extended region of the Iz phase intervening between FM and ZZ.

IV. DMRG SCANS FOR THE FULL XXZ J_1^Δ–J_3^Δ MODEL

In Fig. S4, we show DMRG J_3-scans that are used to construct the phase diagram of the J_1^Δ–J_3^Δ model in Fig. 5 of the main text. While the $\Delta=0.5$ scan looks somewhat similar to the scan for the same Δ in Fig. S3, it has a direct FM-ZZ transition at $J_3=0.30$, with the separate non-scan calculations showing no sign of the intermediate phase.

In the $\Delta=0.25$ and $\Delta=0$ scans, an intermediate region is suggested with the suppressed ordered moments. As we discuss next, initial non-scans in these regions have shown strongly anisotropic correlations, with short correlations

in one direction and FM-like in the other, resembling the state that has been hypothesized as a spin liquid in Ref. [1]. Upon closer inspection and finite-size scaling, they reveal a narrow region of the Iz phase. For $\Delta=0$, $J_3=0.33$ is in the FM phase, $J_3=0.37$ is in the ZZ phase, and $J_3=0.35$ is in the Iz phase by that analysis, confining the Iz phase between $J_3=0.34$ and 0.36. For $\Delta=0.25$, the Iz phase is even narrower, between $J_3=0.315$ and 0.325.

While the Iz phase in the XY limit ($\Delta=0$) of the full XXZ J_1^Δ–J_3^Δ model has been suggested in Ref. [2], the J_3-width of it in our analysis is an order of magnitude narrower than in the results of the pseudo-fermion functional renormalization group method used in Ref. [2].

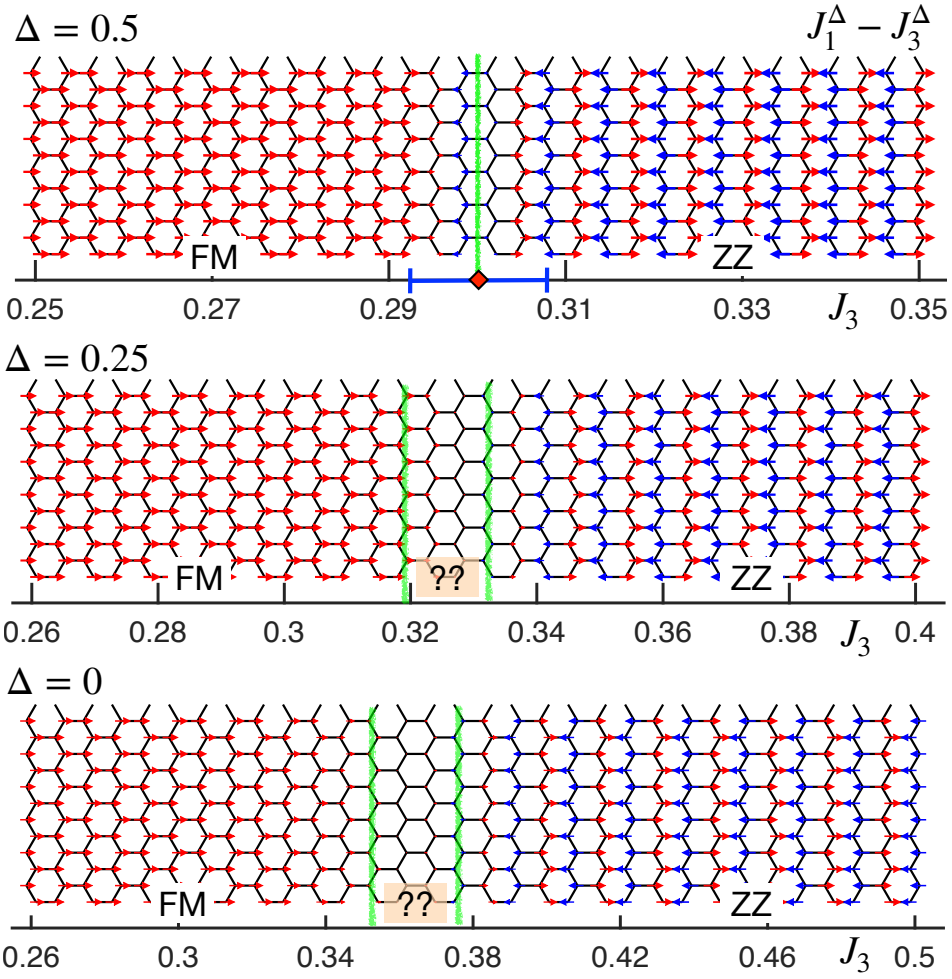

FIG. S4. DMRG J_3-scans in the J_1^Δ–J_3^Δ model for Δ=0.5, 0.25, and 0 on the 12×32 cylinders.

V. PSEUDO-SPIN-LIQUID STATE

In some of the transition regions discussed above for both versions of the XXZ J_1–J_3 model, we have found regimes that can be taken as evidence for a spin-liquid state, similar to the ones reported in Ref. [1]. These include nearly zero ordered moment at intermediate bond dimension in DMRG calculations, for which the system is expected to spontaneously break symmetry if it has an order, and the short-range spin-spin correlation in one direction, as shown in Figs. S5(a) and S5(b). This anisotropy in correlations is suspicious, however, as one would expect a "lock in" of such 1D-like correlations into some order in a larger system. Indeed, with the increase of the system's width, one of the spin-liquid possibilities in the J_1^Δ–J_3 model ($\Delta=0.4$), develops a ZZ order, see Fig. S5(c).

Another such suspect region is in the J_1^Δ–J_3^Δ model, $\Delta=0.25$, near $J_3=0.32$, similar to the one reported in Ref. [1], but it does not follow that trend. In fact, as is shown in Fig. S5(d), the spin-liquid candidate looks even more realistic (less anisotropic) in the YC lattice. However, the system was tested with various boundary conditions and responded strongly to the staggered pinning field $(-1)^i h S_i^z$, developing a substantial Iz order, see Fig. S5(e), with the ordered moment nearly constant $\langle S\rangle\approx 0.1$ in the bulk. Following Ref. [3], we carry out an $1/L_y$-scaling of the ordered moment, which gives a strong indication of the Iz order in the thermodynamic limit, see Fig. S5(f).

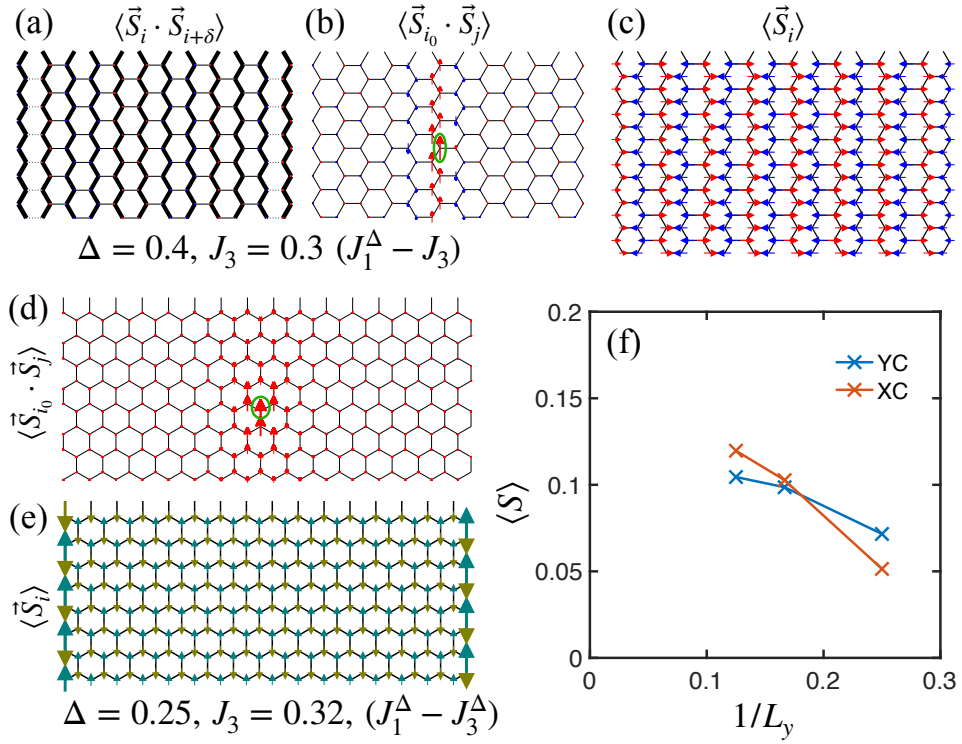

FIG. S5. (a) and (b) 12×12 XC cylinder non-scans for $\Delta = 0.4$ and $J_3 = 0.3$ in the J_1^Δ–J_3 model showing: (a) nearly-zero ordered moment and nearest-neighbor $\langle \vec{S}_i \cdot \vec{S}_{i+\delta} \rangle$ (thickness of the bond), and (b) spin-spin correlation $\langle \vec{S_{i_0}} \cdot \vec{S_j} \rangle$, denoted by the length and direction of the arrow, with i_0 site shown by the green oval. The arrow on i_0 is of length 0.25. (c) Same as (a) on the 16×16 cylinder. (d) Same as (b) on the 8×32 YC cylinder for $\Delta = 0.25$ and $J_3 = 0.32$ in the J_1^Δ–J_3^Δ model. (e) Ordered moment in (d) under the Iz pinning field of 0.5 on both edges. (f) The $1/L_y$-scaling of the Iz ordered moment in the center of the cylinder with the edge pinning fields from (e) and the XC and YC cylinders having the aspect ratio 2, which mimics the 2D limit closely—see Ref. [3].

VI. DMRG RESULTS FOR THE J_1^Δ-J_2^Δ MODEL

Ref. [2] has studied the J_1–J_2–J_3 XXZ model, demonstrating a potentially richer structure of its phase diagram compared to the J_1–J_3 model investigated in our work. Specifically, it was suggested that the spin-liquid phase in the isotropic Heisenberg limit is stable in a much wider region along the J_1–J_2 axis than along the J_1–J_3 axis, with a specific point $J_2 = 0.18$ studied in more detail. In that work, an XXZ cut of the J_1^Δ–J_2^Δ model along the Δ-axis for $J_2 = 0.18$ (and $J_3 = 0$) was also investigated, and a transition to an incommensurate phase from an SL phase was identified near the Heisenberg limit, at $\Delta = 0.96$, with a wide range of the incommensurate phase extending down to the low values of Δ.

Here we briefly present our additional results for the J_1^Δ–J_2^Δ model for this specific choice of $J_2 = 0.18$ and $J_3 = 0$, thus extending our work in a different region of the parameter space. The summary of our results is the following. We do not find any evidence for a spin-liquid state in the Heisenberg limit of this model, and find a double-zigzag state instead. This is similar to our results for the dZZ state in the J_1–J_3 model, found instead of the SL state suggested in Ref. [2], as is discussed in the main text. For the 1D phase diagram along the Δ-axis for the same choice of $J_2 = 0.18$ and $J_3 = 0$, we find two transitions, one at $\Delta = 0.93(2)$ and the other at $\Delta = 0.86(2)$. The lower one is a transition to a FM state, with no sign of the incommensurate phase. While the existence of a transition at $\Delta = 0.93(2)$ is, ideologically, in agreement with the transition found in Ref. [2], in our case it is between a dZZ phase and a potentially novel triple-zigzag state that also has a significant modulation of spins, characteristic of that of the spin-density wave (SDW). We refer to it as to tZZ-SDW state.

The numerical results to substantiate these findings are presented in Fig. S6. The Fig. S6(a) part shows a scan calculation at J_2=0.18 vs Δ from the Heisenberg limit down to $\Delta = 0.8$. The double zigzag phase at the isotropic limit ($\Delta = 1.0$) evolves into a FM state via an intermediate phase. The non-scan calculations in Fig. S6(b) and Fig. S6(d) confirm the dZZ and the FM phases at the respective ends of the scan, with both exhibiting a robust order. The non-scan for the intermediate phase at $\Delta = 0.9$ in Fig. S6(c) retains the characteristics of the SDW state, as the spin's magnitude is not varied in a fashion that would be consistent with a "simple" triple-zigzag phase. While it is possible that the SDW variation may be an artifact of the finite cluster as the tZZ phase has a large unit cell, the dZZ phase in the J_1–J_3 case is much more symmetric and we believe that the observed SDW variation is genuine.

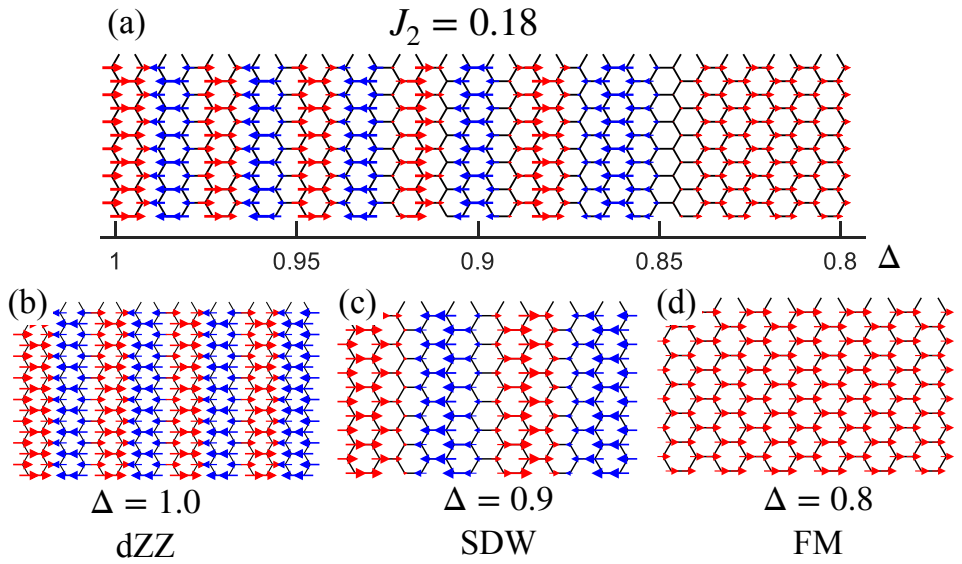

FIG. S6. Results for the J_1^{Δ}–J_2^{Δ} model for $J_2 = 0.18$. (a) DMRG scan on 12×32 cylinder vs Δ, and (b), (c), and (d) are non-scans on 16×16 and 12×12 cylinders for three representative values of Δ.

Lastly, we note that in the energy comparison for the J_1–J_3 Heisenberg case discussed in the main text and shown in Fig. 3(b), we have also investigated a stability of the triple-ZZ state. The tZZ did come very close near the FM-dZZ boundary, but did not become the ground state in that limit. In that sense, the stabilization of the tZZ phase, or a descendant of it, in a different part of the phase diagram does not come as a complete surprise.

VII. GENERALIZED $J_1^{\Delta_1}$-$J_3^{\Delta_3}$ MODEL FOR $BaCo_2(AsO_4)_2$

As is mentioned in the main text, extensive experimental and theoretical searches for the Kitaev magnets on the honeycomb lattice have recently expanded to the Co^{2+}, $S_{eff} = 1/2$ materials. Among this family, $BaCo_2(AsO_4)_2$ has received significant attention [4–8]. Its minimal model description has currently coalesced to a generalized XXZ FM-AFM $J_1^{\Delta_1}$–$J_3^{\Delta_3}$ model [1, 4, 7, 8] with additional Kitaev-like bond-dependent terms.

One such model parametrization was advocated in Ref. [4], based on fitting experimental excitation spectrum in high fields and assuming the spin-spiral ground state with a nearly commensurate ordering **Q**-vector in zero field. Leaving the correctness of the latter assumption aside [6], the model parameters in Ref. [4] were constrained to match the ordering **Q**-vector of the planar spin spiral from the *classical* solution of the generalized XXZ $J_1^{\Delta_1}$–$J_3^{\Delta_3}$ model.

Since we find that such a spiral state does not survive at all in the *quantum* $S = 1/2$ version of the XXZ J_1–J_3 model, as it is overtaken by the collinear phases due to quantum fluctuations, we have checked the validity of the key assumption made in Ref. [4] regarding the structure of the ground state for their proposed set of parameters. The model used in Ref. [4] has strong XXZ anisotropies for the J_1 and J_3 terms, but of different sign, $\Delta_1 \approx 0.16$ and $\Delta_3 = -0.34$, and the ratio $J_3/J_1 \approx -0.33$ (see Eq. [13] of Ref. [4]). The model also contains two minimal bond-dependent corrections in the J_1 exchange matrix.

We have performed DMRG calculations for these parameters, including the bond-dependent terms, on a 12×12

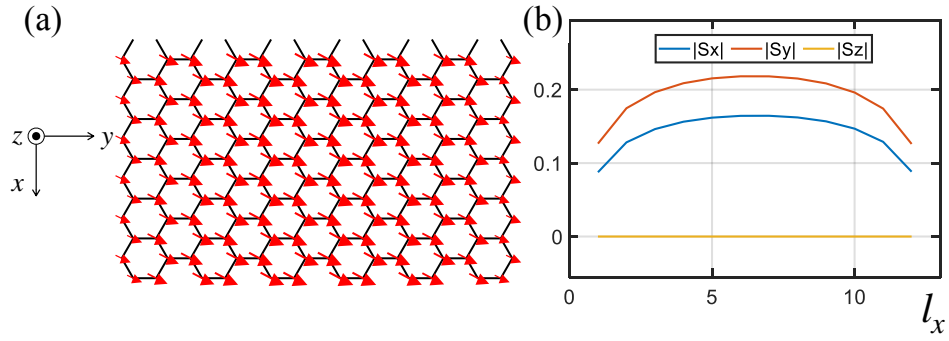

FIG. S7. (a) Spin pattern in the 12×12 DMRG cylinder and (b) spin components in the ground state of the generalized XXZ $J_1^{\Delta_1}$-$J_3^{\Delta_3}$ model model from Ref. [4].

cylinder in order to see whether the opposite sign of Δ_1 and Δ_3, or the bond-dependent terms, are able to stabilize the spiral state to avoid the fate we find for it in the other models. As is shown in Fig S7, we find an FM ground state instead of the spiral state, suggesting that the model parameters for $BaCo_2(AsO_4)_2$ proposed in Ref. [4] are not adequate to describe its ground-state spin configuration and require a reconsideration.

VIII. MINIMALLY AUGMENTED SPIN WAVE THEORY

The spin-wave approach is based on the $1/S$-expansion about a classical ground state of a spin model using bosonic representation for spin operators [9]. Since the classical energy is at a minimum, the first non-zero term of the expansion is quadratic (harmonic), yielding the liner spin-wave theory (LSWT) Hamiltonian in a standard form

$$\mathcal{H} = E_{cl} + \frac{1}{2}\sum_{\mathbf{q}} \left(\hat{\mathbf{x}}^\dagger_{\mathbf{q}} \hat{\mathbf{H}}_{\mathbf{q}} \hat{\mathbf{x}}_{\mathbf{q}} - \frac{1}{2}\mathrm{tr}(\hat{\mathbf{H}}_{\mathbf{q}}) \right) + O(S^0), \qquad \hat{\mathbf{H}}_{\mathbf{q}} = \begin{pmatrix} \hat{\mathbf{A}}_{\mathbf{q}} & \hat{\mathbf{B}}_{\mathbf{q}} \\ \hat{\mathbf{B}}^\dagger_{\mathbf{q}} & \hat{\mathbf{A}}^*_{-\mathbf{q}} \end{pmatrix}, \tag{1}$$

where E_{cl} is the classical energy, $O(S^2)$, $\hat{\mathbf{x}}^\dagger_{\mathbf{q}} = \left(\hat{\mathbf{a}}^\dagger_{\mathbf{q}}, \hat{\mathbf{a}}_{-\mathbf{q}}\right)$ is a vector of the bosonic creation and annihilation operators, and $\hat{\mathbf{H}}_{\mathbf{q}}$ is the Hamiltonian matrix, $O(S)$, in this basis. The diagonalization of $\hat{\mathbf{g}}\hat{\mathbf{H}}_{\mathbf{q}}$, where $\hat{\mathbf{g}}$ is the diagonal para-unitary matrix, yields the LSWT magnon eigenenergies $\{\varepsilon_{1\mathbf{q}}, \varepsilon_{2\mathbf{q}}, \dots, -\varepsilon_{1-\mathbf{q}}, -\varepsilon_{2-\mathbf{q}}, \dots\}$ [10] that are *guaranteed* to be positive definite because the expansion is around a minimum of the classical energy.

From that, the energy of the ground state to the order $O(S)$ is $\mathcal{E} = E_{cl} + \delta E$, where δE is the $1/S$ quantum correction

$$\delta E = \frac{1}{2}\sum_{\mathbf{q}} \Big(\sum_{\alpha} \varepsilon_{\alpha\mathbf{q}} - \mathrm{tr}(\hat{\mathbf{A}}_{\mathbf{q}}) \Big). \tag{2}$$

When the classical state stops being a minimum as some parameter of the model is varied, the quadratic Hamiltonian in (1) ceases to be positive definite, with some of the $\varepsilon^2_{\alpha\mathbf{q}}$ turning negative for some momenta $\mathbf{q}$, and the quantum correction in (2) becoming ill-defined. This hinders the use of the LSWT outside the classical region of stability of a state and limits its ability to describe the shift of the phase boundaries between classical states due to quantum effects and the appearance of the ordered phases that are not favored classically but stabilized in a quantum case.

The resolution to this general conundrum that has plagued application of the SWT to the classically unstable states was suggested in Refs. [11–13]. The method consists of adding a local field term to the Hamiltonian, $\delta\mathcal{H} = \mu \sum_i a^\dagger_i a_i$ (see the main text) and referred to as the *minimally augmented SWT* (MAGSWT). The minimal value of this field is chosen from the condition that all eigenvalues $\varepsilon^2_{\alpha\mathbf{q}}$ are positive definite for all the momenta $\mathbf{q}$.

A. LSWT for the phases of the J_1–J_3 model

The classical energies of the collinear phases of interest per number of atomic unit cells N_A are given by

$$E^{\mathrm{FM}}_{cl} = -3S^2(1 - J_3), \quad E^{\mathrm{ZZ}}_{cl} = -S^2(1 + 3J_3), \quad E^{\mathrm{Iz}}_{cl} = 3S^2(\Delta_1 - J_3\Delta_3), \quad E^{\mathrm{dZZ}}_{cl} = -2S^2, \tag{3}$$

valid for any J_3 and $\Delta_{1(3)}$ of the model (1) of the main text, inside or outside the phase's stability region.

Of the five phases in Fig. 1 of the main text, the magnetic unit cell in the FM and Iz phases is naturally that of the honeycomb lattice (two sites), while for the ZZ and Sp ones it can be reduced to that by the staggered or rotated reference frames, respectively, resulting in the 4×4 Hamiltonian LSWT matrix $\hat{\mathbf{H}}_{\mathbf{q}}$ (1) in all four cases. For the dZZ phase, the staggered reference frame reduces the unit cell from eight to four sites and yields the 8×8 LSWT matrix.

The LSWT treatment of the collinear phases is rather standard and we do not elaborate on it except for a few details. In all two-sublattice cases, FM, ZZ, Iz, and Sp, the LSWT matrices $\hat{\mathbf{A}}_{\mathbf{q}}$, $\hat{\mathbf{B}}_{\mathbf{q}}$ in (1) assume the same structure, for which the eigenvalues of the 4×4 Hamiltonian matrix can be found analytically. One can find additional simplifications of the eigenvalue problem for the FM and Iz phases, and in all four cases in the limit $\Delta_{1(3)} = 0$, see also Ref. [14] for the limiting cases for the Sp phase.

In the 4-sublattice dZZ case, the eigenvalue problem for the 8×8 matrix is not reducible to a compact analytical form. However, analytical solutions are available for the eigenenergies at the high-symmetry $\mathbf{q} = 0$ and $\mathbf{q} = (0, \pi/\sqrt{3})$ points in the Heisenberg limit, which are instrumental for finding the MAGSWT parameter μ.

B. Finding μ in MAGSWT

In the FM, ZZ, and Iz phases, the search for the minimal value of μ for the MAGSWT follows a similar pattern. In a simplified case, such as full XXZ ($\Delta_1 = \Delta_3$) or XY limits, analytical expression for the lowest branch $\varepsilon^2_{1\mathbf{q}}$ simplifies sufficiently to yield the J_3-dependence of the offending negative minimum that needs to be lifted up by a positive shift. The required energy shift is easily related to μ with the Δ-dependence of μ either absent or following trivially

from the considered limiting cases. The resulting solutions correspond to a change of the diagonal matrix element $A \to \bar{A}$ of the LSWT matrix $\hat{\mathbf{A}}_{\mathbf{q}}$, with $\bar{A}$ *in all three cases* given by

$$\bar{A} = A + \mu = 3S\,|\bar{\gamma}_{\mathbf{Q}_{\max}}|\,, \quad \text{where} \quad \bar{\gamma}_{\mathbf{q}} = \gamma_{\mathbf{q}} - J_3\gamma^{(3)}_{\mathbf{q}}, \tag{4}$$

with the first- and third-neighbor hopping amplitudes $\gamma_{\mathbf{q}} = \frac{1}{3}\sum_\alpha e^{i\mathbf{q}\boldsymbol{\delta}_\alpha}$ and $\gamma^{(3)}_{\mathbf{q}} = \frac{1}{3}\sum_\alpha e^{i\mathbf{q}\boldsymbol{\delta}^{(3)}_\alpha}$, and $\mathbf{Q}_{\max}$ defined as

$$\mathbf{Q}_{\max} = \begin{cases} (0,0), & J_3 < J_{3,c1} = 0.25, \\ (Q_x, 0),\ Q_x = \frac{2}{3}\cdot\arccos\left(\frac{1}{2J_3}\cdot\frac{1-3J_3}{1-2J_3}\right), & J_{3,c1} < J_3 < J_{3,c2}, \\ (2\pi/3, 0), & J_3 > J_{3,c2} = (\sqrt{17}-1)/8 \approx 0.3904, \end{cases} \tag{5}$$

Technically, the condition for the maximum of $|\bar{\gamma}_{\mathbf{q}}|$ is related to that of the classical energy minimum in the Sp phase.

Interestingly, the resultant MAGSWT spectrum in the Iz phase and the quantum energy correction (2) that derives from it, are fully independent of the anisotropy parameters Δ_n.

In the dZZ case, the search of μ has involved analysis of the spectrum obtained by a numerical diagonalization of the $\left(\hat{\mathbf{g}}\hat{\mathbf{H}}_{\mathbf{k}}\right)^2$ matrix in the Heisenberg limit, which helped in identifying the relevant high-symmetry $\mathbf{q}$ points that require stabilization corrections. The diagonalization at these points can be reduced to an analytical form, which, in turn, yields the minimal value of μ. In a narrow region of $0.1892 < J_3 < 0.2030$, the two lowest unstable branches trade places and, in a row, develop negative minima at small but finite $\mathbf{q}$'s. For that region, we find that a straightforward linear interpolation for μ between the analytic solutions from the neighboring regions is the most effort-effective, as it stabilizes the spectrum if not with zero but with a very small gap. The resultant explicit expressions for μ are

$$\mu = \begin{cases} S\left(\sqrt{5-2J_3+J_3^2}-1-3J_3\right), & J_3 < \widetilde{J}_{c1} = 0.1892, \\ \text{interpolate}, & \widetilde{J}_{c1} < J_3 < \widetilde{J}_{c2} = 0.203, \\ 2S\left(\sqrt{2-2J_3+J_3^2}-1\right), & \widetilde{J}_{c2} < J_3 < \widetilde{J}_{c3} = 0.25, \\ 2SJ_3, & J_3 > \widetilde{J}_{c3}. \end{cases} \tag{6}$$

As in the other coplanar phases, FM and ZZ, μ is independent of the XXZ anisotropies Δ_n.

C. Energies

Following the MAGSWT strategy, quantum corrections to the groundstate energies in all competing phases can now be calculated in a conventional $1/S$ fashion using Eq. (2) with the expressions for the minimal chemical potential from (4) and (6). Then the total energies $\mathcal{E}(J_3, \Delta)$ can be compared between the phases to create the phase diagram.

Figure S8(a) shows the J_3 energy-cuts in the Heisenberg limit, $\Delta_{1(3)} = 1$, of the J_1–J_3 model. The dashed lines are classical energies (3) and solid lines are energies with quantum corrections (2). The vertical dashed lines are classical FM-Sp and Sp-ZZ boundaries, $J_{3,c1}$ and $J_{3,c2}$. The dotted line is the intersection of the FM and ZZ classical energies,

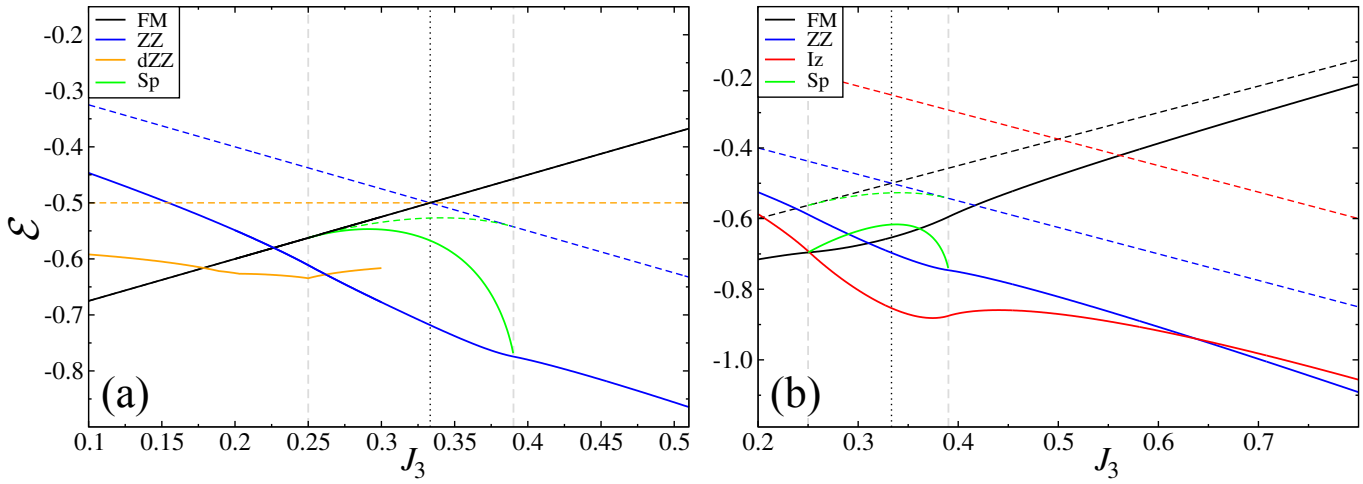

FIG. S8. (a) The classical (dashed lines) and quantum (solid lines, from (2)) energies of the FM, ZZ, Sp, and dZZ states vs J_3 for $\Delta_{1(3)} = 1$ per atomic unit cell. The vertical dashed lines are classical FM-Sp and Sp-ZZ boundaries and the dotted line is the crossing of E_{cl} for the FM and ZZ states. (b) Same as (a) for the FM, ZZ, Sp, and Iz states for $\Delta_1 = 0$ and $\Delta_3 = 1$.

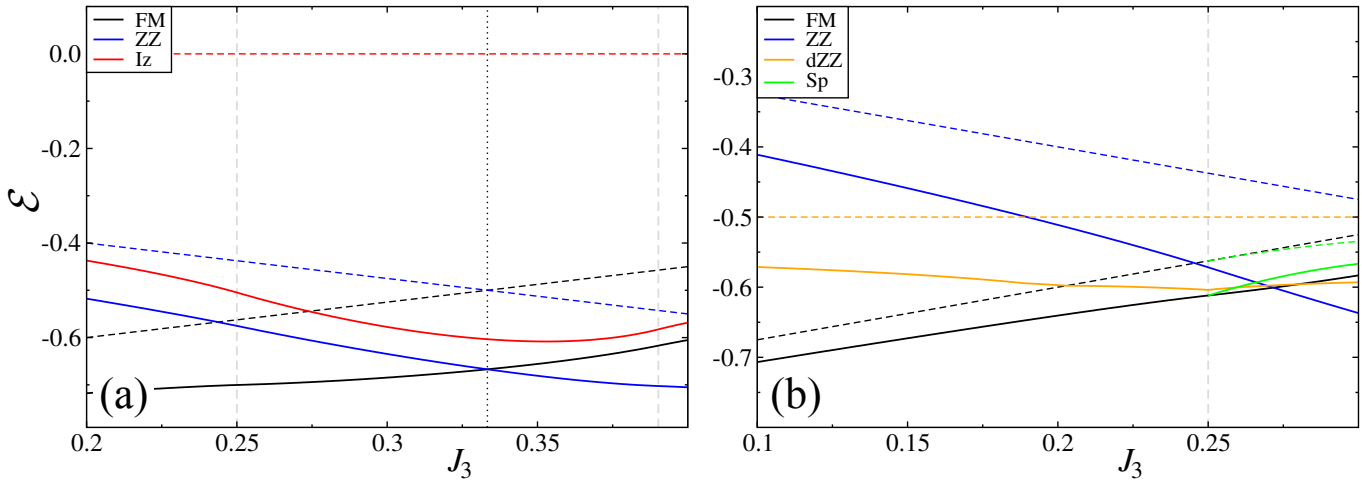

FIG. S9. (a) Same as in Fig. S8(b) for the FM, ZZ, and Iz states in the "full" XY limit, $\Delta_1 = \Delta_3 = 0$. (b) Same as in Fig. S8(a) for the FM, ZZ, Sp, and dZZ states for $\Delta_1 = 0.5$ and $\Delta_3 = 1$.

$J_3 = 1/3$. The Iz phase is not competitive. The Sp phase uses standard SWT with no augmenting as it is stable through its extent. The FM is an exact eigenstate, so the quantum corrections to it are zero.

The first effect is the expansion of the ZZ phase (blue lines). While the FM is fluctuation-free, the ZZ is not, which pushes its energy down and the crossing with the FM's energy below the $J_{3,c1}$ point where the FM is unstable classically, superseding the non-collinear Sp phase, which is not effective in lowering its energy. However, near $J_{3,c1}$ another collinear phase, dZZ, is competitive, making it a ground state in a finite range of J_3 (orange lines).

One can note a very close agreement of the MAGSWT dZZ-ZZ transition at $J_3 = 0.262$ compared to the DMRG value of 0.26. On the other hand, the FM-dZZ transition is at a lower $J_3 = 0.1785$ than the DMRG one at $J_3 \approx 0.24$. One can ascribe this difference to a larger sensitivity of the MAGSWT phase boundaries to the higher-order corrections in this case because FM state is non-fluctuating in the Heisenberg limit.

For the "partial" XY limit, with $\Delta_1 = 0$ and $\Delta_3 = 1$, see Figure S8(b). In this case, dZZ is not competitive, but Iz is. All phases are fluctuating in this limit, including FM. The Sp phase is not effective in benefiting from quantum fluctuations. The transition point between FM and ZZ phase is renormalized to a slightly smaller J_3 from its classical value. However, both are overtaken by the strongly-fluctuating Iz phase in a wide window of J_3. One observation is that while the FM-Iz transition is associated with a rather steep energy crossing, the Iz-ZZ crossing is rather shallow, suggesting stronger higher-order effects on the MAGSWT phase boundary for the latter, but not the former. This is in accord with the numerical values: $J_3 \approx 0.269(15)$ [DMRG] vs 0.2513 [MAGSWT] for the FM-Iz boundary and $J_3 \approx 0.554(23)$ [DMRG] vs 0.637 [MAGSWT] for the Iz-ZZ boundary. Similar discrepancies for the finite Δ_1 in the phase diagram in Fig. 1(b) of the main text can be attributed to the same effect.

We note that in the "partial" XY case in Fig. S8(b), the Heisenberg J_3-term helps to stabilize the Iz state. The effect of the Δ_3 anisotropy is tested by the "full" XY limit of the model, in which the benefit of the out-of-plane spin-coupling is absent. The J_3-cut in this limit is shown in Figure S9(a). The Iz phase can be seen as remarkably effective at lowering its energy, with the quantum fluctuation part being about four times of that for the FM and ZZ states. However, while being closely competitive, the Iz phase is not stable in the full XY limit according to MAGSWT. This result is, superficially, in a disagreement with the DMRG, which does show a narrow strip of the Iz phase in Fig. 5 of the main text. Nevertheless, with the energy curves in Fig. S9(a) and Fig. S8(b) in mind, it is clear that the MAGSWT misses Iz phase in the full XY limit only slightly.

An additional J_3-cut for $\Delta_1 = 0.5$ and Heisenberg J_3 is shown in Fig. S9(b). Here, the competing phases are the same as in Fig. S8(a), with the dZZ phase coming extremely close, but not able to stabilize, yielding a direct FM-ZZ transition for this value of Δ_1. This is in a close agreement with DMRG, which shows a narrow dZZ slice for J_3 between 0.280(4) and 0.290(6) at this Δ_1, with the FM-ZZ transition being direct for the next cut at $\Delta_1 = 0.4$, see Fig. 1(b) of the main text. Given the energy differences in Fig. S9(b), the agreement is indeed very close.

Such additional insights into the energetics of the competing phases are instrumental for the understanding of their competition. They also underscore the undeniable success of the MAGSWT in describing classically unstable states.

[1] A. Bose, M. Routh, S. Voleti, S. K. Saha, M. Kumar, T. Saha-Dasgupta, and A. Paramekanti, Proximate Dirac spin liquid in the J_1-J_3 XXZ model for honeycomb cobaltates, arXiv:2212.13271 (2022).

[2] Y. Watanabe, S. Trebst, and C. Hickey, Frustrated Ferromagnetism of Honeycomb Cobaltates: Incommensurate Spirals, Quantum Disordered Phases, and Out-of-Plane Ising Order, arXiv:2212.14053 (2022).

[3] S. R. White and A. L. Chernyshev, Neél Order in Square and Triangular Lattice Heisenberg Models, Phys. Rev. Lett. **99**, 127004 (2007).

[4] T. Halloran, F. Desrochers, E. Z. Zhang, T. Chen, L. E. Chern, Z. Xu, B. Winn, M. Graves-Brook, M. B. Stone, A. I. Kolesnikov, Y. Qiu, R. Zhong, R. Cava, Y. B. Kim, and C. Broholm, Geometrical frustration versus Kitaev interactions in $BaCo_2(AsO_4)_2$, Proc. Natl. Acad. Sci. U.S.A. **120**, e2215509119 (2023).

[5] R. Zhong, T. Gao, N. P. Ong, and R. J. Cava, Weak-field induced nonmagnetic state in a Co-based honeycomb, Sci. Adv. **6**, eaay6953 (2020).

[6] L.-P. Regnault, C. Boullier, and J. Lorenzo, Polarized-neutron investigation of magnetic ordering and spin dynamics in $BaCo_2(AsO_4)_2$ frustrated honeycomb-lattice magnet, Heliyon **4**, e00507 (2018).

[7] S. Das, S. Voleti, T. Saha-Dasgupta, and A. Paramekanti, XY magnetism, Kitaev exchange, and long-range frustration in the $J_{\text{eff}} = \frac{1}{2}$ honeycomb cobaltates, Phys. Rev. B **104**, 134425 (2021).

[8] P. A. Maksimov, A. V. Ushakov, Z. V. Pchelkina, Y. Li, S. M. Winter, and S. V. Streltsov, Ab initio guided minimal model for the "Kitaev" material $BaCo_2(AsO_4)_2$: Importance of direct hopping, third-neighbor exchange, and quantum fluctuations, Phys. Rev. B **106**, 165131 (2022).

[9] T. Holstein and H. Primakoff, Field dependence of the intrinsic domain magnetization of a ferromagnet, Phys. Rev. **58**, 1098 (1940).

[10] J. Colpa, Diagonalization of the quadratic boson hamiltonian, Physica A: Statistical Mechanics and its Applications **93**, 327 (1978).

[11] S. Wenzel, T. Coletta, S. E. Korshunov, and F. Mila, Evidence for Columnar Order in the Fully Frustrated Transverse Field Ising Model on the Square Lattice, Phys. Rev. Lett. **109**, 187202 (2012).

[12] T. Coletta, M. E. Zhitomirsky, and F. Mila, Quantum stabilization of classically unstable plateau structures, Phys. Rev. B **87**, 060407(R) (2013).

[13] T. Coletta, S. E. Korshunov, and F. Mila, Semiclassical evidence of columnar order in the fully frustrated transverse-field Ising model on the square lattice, Phys. Rev. B **90**, 205109 (2014).

[14] E. Rastelli, A. Tassi, and L. Reatto, Non-simple magnetic order for simple Hamiltonians, Physica B+C **97**, 1 (1979).